

Independent effects of structural optimization and resveratrol functionalization on extracellular matrix scaffolds for bone regeneration

Bowen Li^{a,b}, Mei Wang^a, Yuhua Liu^{a,*}, Yongsheng Zhou^{a,*}, Lin Tang^a, Pengyue You^a, Yi Deng^a

^a Department of Prosthodontics, Peking University School and Hospital of Stomatology & National Center of Stomatology & National Clinical Research Center for Oral Diseases & National Engineering Laboratory for Digital and Material Technology of Stomatology & Central Laboratory, Peking University School and Hospital of Stomatology, Beijing 100081, PR China

^b Department of Stomatology, Beijing Hospital, National Center of Gerontology, National Health Commission, Institute of Geriatric Medicine, Chinese Academy of Medical Science, Beijing 100730, China

ARTICLE INFO

Keywords:

Bone tissue engineering
Scaffold
Extracellular matrix
Small intestinal submucosa
Resveratrol

ABSTRACT

Due to their natural biological activity and low immunogenicity, decellularized extracellular matrix (ECM) materials have aroused interest as potential scaffold materials in tissue engineering. Decellularized small intestinal submucosa (SIS) is one ECM biomaterial that can be easily sourced. In the present study, we tested whether the osteogenesis of SIS scaffolds was enhanced via structural optimization and resveratrol (RSV) functionalization and explored the independent effects of these modifications. We obtained SIS scaffolds with different pore structures by controlling the preparation concentration. The group with superior osteogenic properties was further RSV-functionalized via covalent immobilization. We conducted a series of *in vitro* and *in vivo* studies to explore the effects of these two optimization strategies on the osteogenic properties of SIS scaffolds. The results showed that pore structure and RSV functionalization significantly affected the osteogenic properties of SIS scaffolds. With a fabrication concentration of 1%, the SIS scaffolds had superior osteogenic properties. Through covalent coupling, RSV was successfully grafted onto SIS scaffolds, where it was slowly released. The most significant improvements in osteogenic properties were obtained with a coupling concentration of 1%. Furthermore, in *in vivo* experiments, vascular and new bone tissue formation was enhanced with RSV/SIS scaffolds compared with SIS scaffolds and the blank control group at 4 weeks after implantation. These findings indicate that the RSV/SIS scaffolds obtained via dual optimization strategies show promise as biomaterials in bone tissue engineering.

1. Introduction

Bone tissue engineering (BTE) is a promising strategy for bone regeneration treatment, in which scaffolds play an indispensable role. Traditional scaffolds are considered carriers of exogenous seed cells [1]. Accordingly, one goal of scaffold-based BTE is to induce endogenous cells that can repair damaged areas [2]. Thus, researchers have emphasized the design and implantation of functional scaffolds instead of non-living scaffolds [3]. Functional scaffolds can mimic the role of the extracellular matrix (ECM) not only by supporting cell growth but also by delivering biological and mechanical cues that trigger cell migration, proliferation and differentiation, thereby generating new, cell-driven functional tissues [3,4]. Hence, the design of functional scaffolds has recently become a research hotspot in the BTE domain [5–7].

Many studies have attempted to identify optimal materials for functional scaffolds. One advantage of a decellularized ECM is that it can maintain and/or guide stem cell differentiation without stimulating the immune response of the host tissue [8,9]. Thus, it is considered a gold-standard for scaffold materials [10]. The ECM can preserve the hierarchical complexity of the natural tissue organization and provide necessary signals to regulate cell function, which are difficult to reproduce in non-native biomaterials [11,12]. Among the different types of ECM components, small intestinal submucosa (SIS) is the most commonly used and has been approved by the Food and Drug Administration. SIS is mainly composed of type I collagen, fibronectin, glycosaminoglycan and some endogenous growth factors, for instance, vascular endothelial growth factor (VEGF) and transforming growth factor β (TGF- β) [13,14]. SIS-based scaffolds have been found to

* Corresponding authors.

E-mail addresses: liuyuhua@bjmu.edu.cn (Y. Liu), kqzhouysh@hsc.pku.edu.cn (Y. Zhou).

<https://doi.org/10.1016/j.colsurfb.2022.112370>

Received 20 October 2021; Received in revised form 17 January 2022; Accepted 23 January 2022

Available online 26 January 2022

0927-7765/© 2022 Elsevier B.V. All rights reserved.

facilitate the adhesion, proliferation and osteogenic differentiation of bone marrow mesenchymal stem cells (BMSCs) [15], thus exhibiting its potential in BTE research. However, the inherent monolayer membrane structure and the microenvironment provided by SIS limit its application in bone regeneration [15–17]. Therefore, designing functional SIS scaffolds with improved osteogenic activity is an urgent issue in BTE.

The physical properties of scaffolds can affect cell behaviour, especially the fate of stem cells, and ultimately affect the outcomes of bone defect repair [18]. Pore structure is one important physical property of scaffolds. Key structural parameters, such as pore size, porosity and interconnectivity, affect bone formation and ingrowth [19]. Micropores may restrict cell migration, as well as the spread of nutrients and the removal of waste, leading to necrotic areas within a structure [20]. In contrast to micropores, macropores provide less surface area, which limits protein adhesion and cell adhesion *in vitro* [21]. Further, they may diminish the mechanical properties of scaffolds [19]. Therefore, customizing physical characteristics by optimizing such structural parameters is essential in the design of functional scaffolds [22]. However, in cases where the tissue around the defect does not have sufficient inherent regeneration potential, the above biological effects are limited unless physical cues are also supplied [23]. Therefore, many studies have used more than one method to improve the osteogenic activity of scaffolds [24–27].

Substantial research efforts have already been focused on the development of functional scaffolds with multiple biomolecules such as drugs and growth factors, with the aim of delivering biological cues to stimulate favourable cellular responses and bone formation [28,29]. These osteoinductive biomolecules can be loaded onto scaffolds *via* physical incorporation, chemical covalent coupling or encapsulation to achieve biological functionalization of the scaffold [3]. Resveratrol (RSV) is a polyphenolic phytoestrogen present in some plants such as grapes and peanuts that has anti-inflammatory, antioxidation and anti-tumour properties [30]. RSV can enhance the proliferation and differentiation of osteoblasts and stimulate new bone regeneration by regulating bone-related signals [31]. The underlying osteogenic mechanism of RSV may include enhancement of the Wnt/ β -catenin signalling pathway, activation of sirtuin 1 and activation of acetylate runt-related transcription factor 2 (RUNX2) [30]. In terms of the biological functionalization of scaffolds, RSV has been used to modify a variety of biomaterials, such as polycaprolactone scaffolds [32], PEEK/nMCS composites [33] and cellulose acetate membranes [34].

Given the considerations detailed above, in the present study, we conducted structural optimization and RSV functionalization while designing an SIS scaffold. For this purpose, we explored the independent effects of these two optimization methods on the osteogenic activity of SIS scaffolds *via* a comprehensive evaluation of the material properties as well as *in vitro* and *in vivo* examinations of osteogenic differentiation. We also assessed the optimal pore structure and RSV coupling concentration. We verified the effectiveness of these two functional strategies through physicochemical characterization, *in vitro* cell experiments and animal experiments, and explored the potential applications of this dually optimized scaffolding material in BTE.

2. Materials and methods

2.1. Scaffold fabrication

2.1.1. SIS scaffolds with different pore structures

SIS scaffolds were fabricated following a previously reported method with some modifications [16]. Briefly, decellularized SIS (Datsing Biological Technology Co., China) was ground into powder using a Freezer/Mill (6770, SPEX Inc., USA) at $-198\text{ }^{\circ}\text{C}$, and the powder was then lyophilized at $-80\text{ }^{\circ}\text{C}$ for 24 h using a freeze dryer (FreeZone, Labconco, USA). The resulting SIS powder was dissolved in deionized water containing pepsin (0.1% w/v) and acetic acid (3% v/v). We used three different concentrations (0.5%, 1% and 2% w/v) to control the pore

structure parameters of the scaffolds. The SIS solutions were stirred for 48 h at $37\text{ }^{\circ}\text{C}$ and then carefully poured into well plates to form cylinders. After pre-freezing for 3 h at $-80\text{ }^{\circ}\text{C}$, the moulds were freeze-dried at $-80\text{ }^{\circ}\text{C}$ and 16.2 atm for 24 h. Afterward, the scaffolds were cross-linked with 1-ethyl-3-(3-dimethylamino propyl) carbodiimide/N-hydroxysuccinimide (EDC/NHS; 50 mM/25 mM) in 95% ethanol for 24 h, washed with deionized water to remove the crosslinker, and freeze-dried to harvest the final SIS scaffolds (hereinafter referred to as 0.5%SIS, 1%SIS and 2%SIS scaffolds).

2.1.2. RSV-functionalized SIS scaffolds

SIS scaffolds functionalized for RSV (referred to as RSV/SIS scaffolds) were prepared using a similar protocol except that we only used 1% SIS solution to fabricate the scaffolds, and RSV (Aladdin, China) was added to EDC/NHS solution at different concentrations (0.1%, 1% or 2% w/v) before crosslinking. These scaffolds are hereinafter referred to as 0.1%RSV/SIS, 1%RSV/SIS and 2%RSV/SIS scaffolds. During the cross-linking process, hydrolysable ester linkages formed between RSV and the SIS scaffolds [35], that is, covalent coupling took place to complete the RSV functionalization process.

2.2. Scaffold characterization

2.2.1. Morphological and structure observations

We assessed the pore morphology of the SIS scaffolds using an environmental scanning electron microscope (ESEM; Quanta 200F, FEI, Netherlands). The ESEM could image non-conductive samples without special sample preparation such as gold coating, which would impact the properties of the samples. Structural features of the scaffolds, such as the pore shape and pore size, were measured using the ImageJ program (NIH, USA).

To study the effects of RSV functionalization on SIS scaffolds, we used the ESEM and the same image analysis method mentioned above to examine the microstructure of the three RSV/SIS scaffolds. The surface structure before and after RSV functionalization was obtained by Fourier transform infrared (FTIR) spectroscopy (Nicoletis 10, Thermo Fisher Scientific, USA) in the wavenumber region from 400 to 4000 cm^{-1} . The functional groups and binding forms of RSV and SIS scaffolds were analyzed according to the characteristic peaks on the FTIR spectra.

2.2.2. Porosity

We determined the porosity of the scaffolds using the liquid displacement method [36]. Briefly, scaffold samples ($n = 5/\text{group}$) were immersed in a known volume (V_0) of anhydrous ethanol for 10 min until they were saturated, and the volume remaining after submersion of the samples was recorded as V_1 . After removing the scaffold, the residual ethanol volume was recorded as V_2 . The porosity (P) of the scaffolds was calculated as follows:

$$P (\%) = \frac{V_0 - V_2}{V_1 - V_2} \times 100\% \quad (1)$$

2.2.3. Water absorption ability

After being weighed (baseline weight = m_0), scaffold samples ($n = 5/\text{group}$) were lowered into distilled water at room temperature. After 2 h, the scaffolds were taken out of the water, and the surfaces were gently wiped with tissue paper to remove the excess liquid. Then, the weights of the samples were measured (m_1). The water absorption ability (W) was calculated thus:

$$W (\%) = \frac{m_1 - m_0}{m_0} \times 100\% \quad (2)$$

2.2.4. *In vitro* degradation

We examined the *in vitro* degradation of the samples by measuring the decrease in weight during the degradation process. Scaffold samples ($n = 5/\text{group}$) were weighed (m_0) and then incubated in a centrifuge

tube containing 20 mL of phosphate-buffered saline (PBS; pH = 7.4) on a shaking table at 37 °C and 80 rpm. After soaking for 1, 2, 3, 5, 7, 10, 14, 21 and 28 days, the samples were removed from the degradation medium, and half of the medium was replaced. The scaffolds were washed several times with deionized water, freeze-dried, and weighed again (m_n). The percentage of weight lost (D) after each time interval for each sample was calculated as follows:

$$D (\%) = \frac{m_0 - m_n}{m_0} \times 100\% \quad (3)$$

2.2.5. Drug loading and in vitro drug release

The maximum absorbance peak of RSV is observed at 306 nm [33]. To explore differences in drug loading among the three types of RSV/SIS scaffolds, each sample was placed in a centrifuge tube containing 1 mL of absolute ethanol, which was then positioned in a constant temperature oscillator for 24 h (37 °C, 80 rpm). We used an ultraviolet spectrophotometer (NanoDrop8000, Thermo, USA) to measure the absorbance at 306 nm (n = 5/group).

To investigate the rate of in vitro drug release, RSV/SIS scaffolds (n = 5/group) were placed in 2 mL of PBS and transferred to a stirring incubator (37 °C, 80 rpm). At specific time points, 1 mL of PBS was removed, and fresh PBS was added. The samples were analysed using an ultraviolet spectrophotometer to measure the absorption maximum of RSV at 306 nm (n = 5/group).

2.3. In vitro cell experiments

2.3.1. Cell culture

Using a previously described method [37], human BMSCs (hBMSCs) were isolated from the alveolar crest of volunteers. The study protocol adhered to the ethical principles and requirements of the Ethics Committee of Peking University Hospital of Stomatology. The hBMSCs were cultured in α -minimum essential medium (GIBCO, USA) with 10% foetal bovine serum (Hyclone, USA) and antibiotics (100 mg/mL streptomycin, 100 U/mL penicillin; Hyclone, USA) at 37 °C in a moist atmosphere with 5% CO₂. The medium was replaced every other day. hBMSCs from passages 4–6 were digested with 0.25% trypsin and then suspended in fresh medium for the following experiments.

2.3.2. Cell proliferation

To evaluate the proliferation of hBMSCs on SIS scaffolds and RSV/SIS scaffolds, approximately 2×10^4 cells were seeded onto the scaffolds in 48-well plates. The growth medium was changed every 2 days. At 1, 3, 5, 7 and 11 days, we used the Cell Counting Kit (CCK)–8 Assay Kit (Donjindo, Japan) to evaluate the number of viable cells. The optical density (OD) was measured at 490 nm using a microplate meter (ELX800, BIOTEK, USA).

2.3.3. Cell viability

The effects of the SIS scaffolds and RSV/SIS scaffolds on cell survival were studied using a LIVE/DEAD kit (KeyGEN BiOTECH, China). The samples were washed with PBS and stained in a solution containing calcein AM and ethidium homodimer-1 for 30 min, then washed again with PBS. The mixtures were subsequently observed under confocal laser scanning microscopy (TCS SP8 X, Leica, Germany). Healthy cells fluoresced in green, whereas the nuclei of dead cells fluoresced in red [38].

2.3.4. Alkaline phosphatase (ALP) staining and activity quantitation

Approximately 4×10^4 cells were seeded onto SIS scaffolds or RSV/SIS scaffolds in 48-well plates containing growth medium. These were incubated for 24 h and then inoculated in osteogenic induction medium (100 nM dexamethasone, 50 μ g/mL ascorbic acid and 10 mM β -glycerophosphate). On days 7 and 14, cell-scaffolds were washed with PBS and fixed in 4% paraformaldehyde for 10 min. Cells were then

Table 1
Primer sequences for real-time qPCR.

Gene	Primers (F = forward, R = reverse)
ALP	F: CTATCCTGGCTCCGTG R: GCTGGCAGTGGTCAGA
RUNX2	F: TGGTTACTGTCATGGCGGGTA R: CCATCCCCTAGGACTCCCA
COL-1	F: AGAGGAAGGAAAAGCGAGGAG R: GGACCAGCAACACCATCTG
BMP-2	F: TGACGAGGTCTGACCGAGTTC R: TGAGTGCCTGCGATACAGGTCTAG
OCN	F: GTGCAGAGTCCAGCAAAGGT R: TCAGCCAACTCGTCACAGTC
ONN	F: TACACCAACCTCTCGTACATCG R: CATGTCTGAAGCGCAGTAAGATT
BSP	F: CAGGCCAGATATTATCTTTACA R: CTCCTCTTCTTCCTCCTCCTC
GAPDH	F: GTTCGAGGACTGGTCCAAA R: GCCAGAGTTAAAAGCAGCC

washed with PBS three times and incubated with ALP staining kit reagents (Cwbiotech, China) at 25 °C in the dark. The samples were then washed three times with distilled water and observed under an inverted microscope (IX73, Olympus, Japan). For ALP activity detection, the cells on the scaffolds were digested with 0.25% trypsin and collected. After that, the cells were lysed with 0.1% Triton X-100 solution for 15 min and then centrifuged at 4 °C and 12,000 rpm for 30 min. The total protein amounts were analysed using a BCA assay (Cwbiotech, China). The reaction solution was added to each test well according to the manufacturer's protocol for the ALP assay kit (Jiancheng, China). Subsequently, the absorbance value (OD value) at 520 nm was detected using a spectrophotometer after 30 min.

2.3.5. Alizarin red S (ARS) staining and quantitation

For the ARS assays, cells were cultured in osteogenic induction medium for 21 days and then fixed in 4% paraformaldehyde for 15 min, followed by staining with ARS solution for 30 min at room temperature. Then, the cell-scaffold mixtures were washed with distilled water and observed under an inverted microscope. Thereafter, mineralized nodules were dissolved with 10% cetylpyridinium chloride (Sigma-Aldrich, USA) for semi-quantitative analysis of absorbance at 562 nm using a spectrophotometer.

2.3.6. Reverse transcription-quantitative PCR (qPCR)

We evaluated the effects of pore structure and RSV functionalization on hBMSC differentiation based on the expression levels of genes involved in osteoblastic differentiation. To this end, we used real-time qPCR. Approximately 1×10^5 cells were cultured on each scaffold in 12-well plates for 7 and 14 days. The qPCR assay was carried out using SYBR Green (Roche, Switzerland) and a real-time PCR system (7500, Applied Biosystems, USA). The qPCR primers used in the experiments are shown in Table 1. The mRNA expression levels of all genes were normalized based on GAPDH as the internal control. Relative expression was calculated using the $2^{-\Delta\Delta CT}$ method [39].

2.3.7. Animal experiments

Sprague-Dawley rats (male, 6–8 weeks old, weighing 300–350 g) were chosen for a critical-size skull defect experiment. All animal surgical procedures were approved by the Animal Research Committee of Peking University Health Science Center. Based on the cell culture results, the 1%SIS scaffolds and 1%RSV/SIS scaffolds were selected for evaluation, and skull defects without scaffolds were used as the blank control group.

The rats were first anesthetized with pentobarbital sodium (50 mg/kg). Two round full-thickness bone defects (5 mm in diameter) were created on each side of the parietal lobe using an electric trephine drill with continuous cooling with sterile 0.9% saline. All rats were randomly

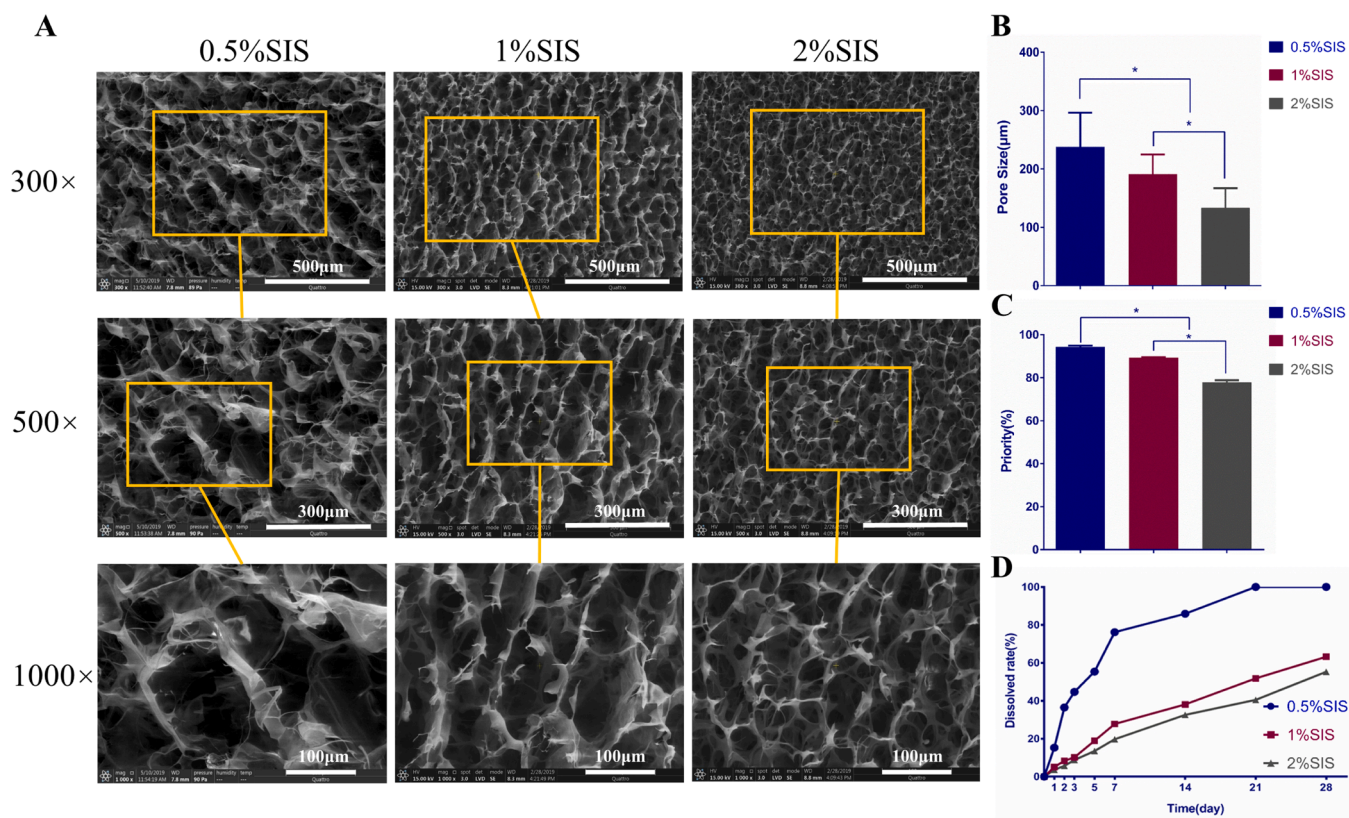


Fig. 1. Characteristics of the SIS scaffolds. (A) ESEM images, (B) pore sizes, (C) porosity and (D) dissolution rates of the different types of scaffolds. *, $P < 0.05$.

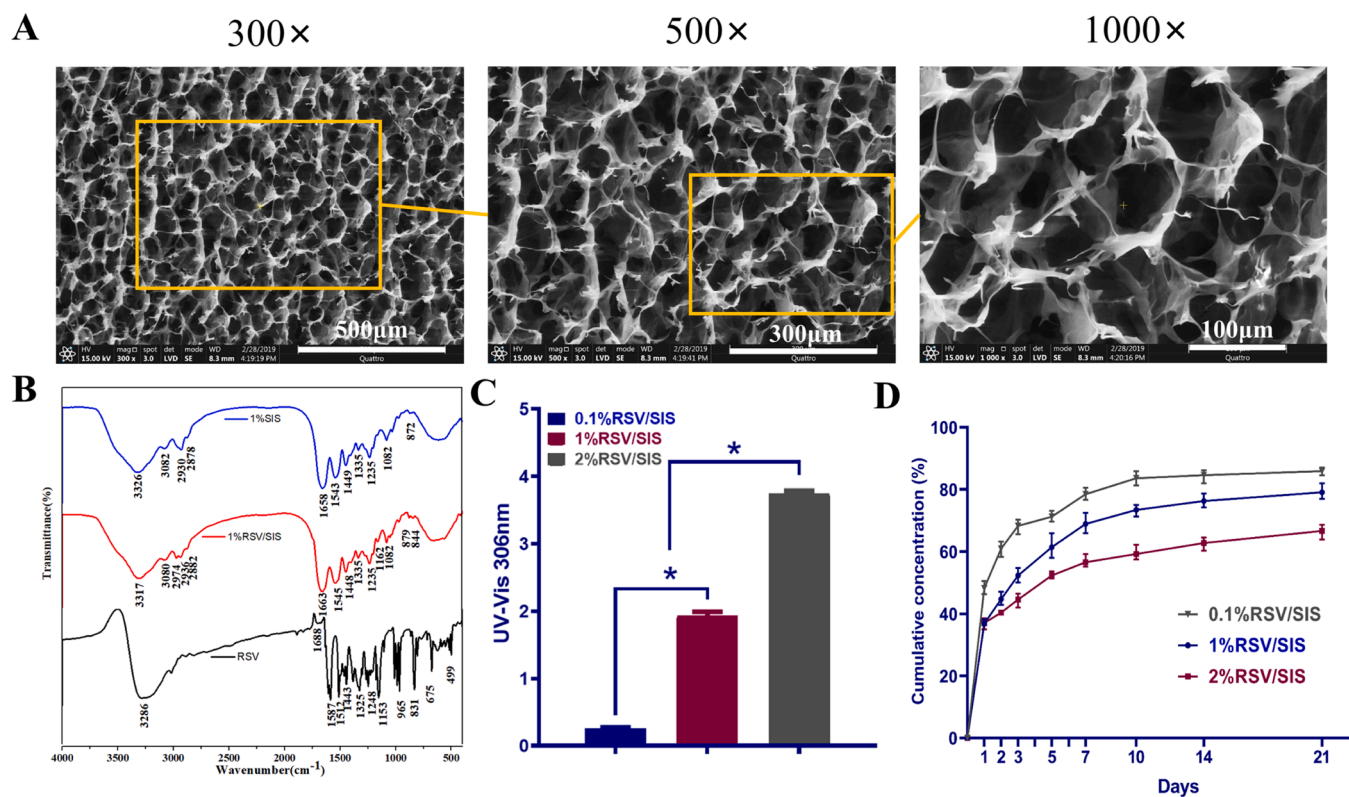


Fig. 2. Characteristics of the RSV/SIS scaffolds. (A) ESEM images of the scaffolds, (B) FTIR spectra of RSV and the scaffolds, (C) relative amounts of drug loaded onto the scaffolds, and (D) the release profile of RSV from the SIS scaffolds. *, $P < 0.05$.

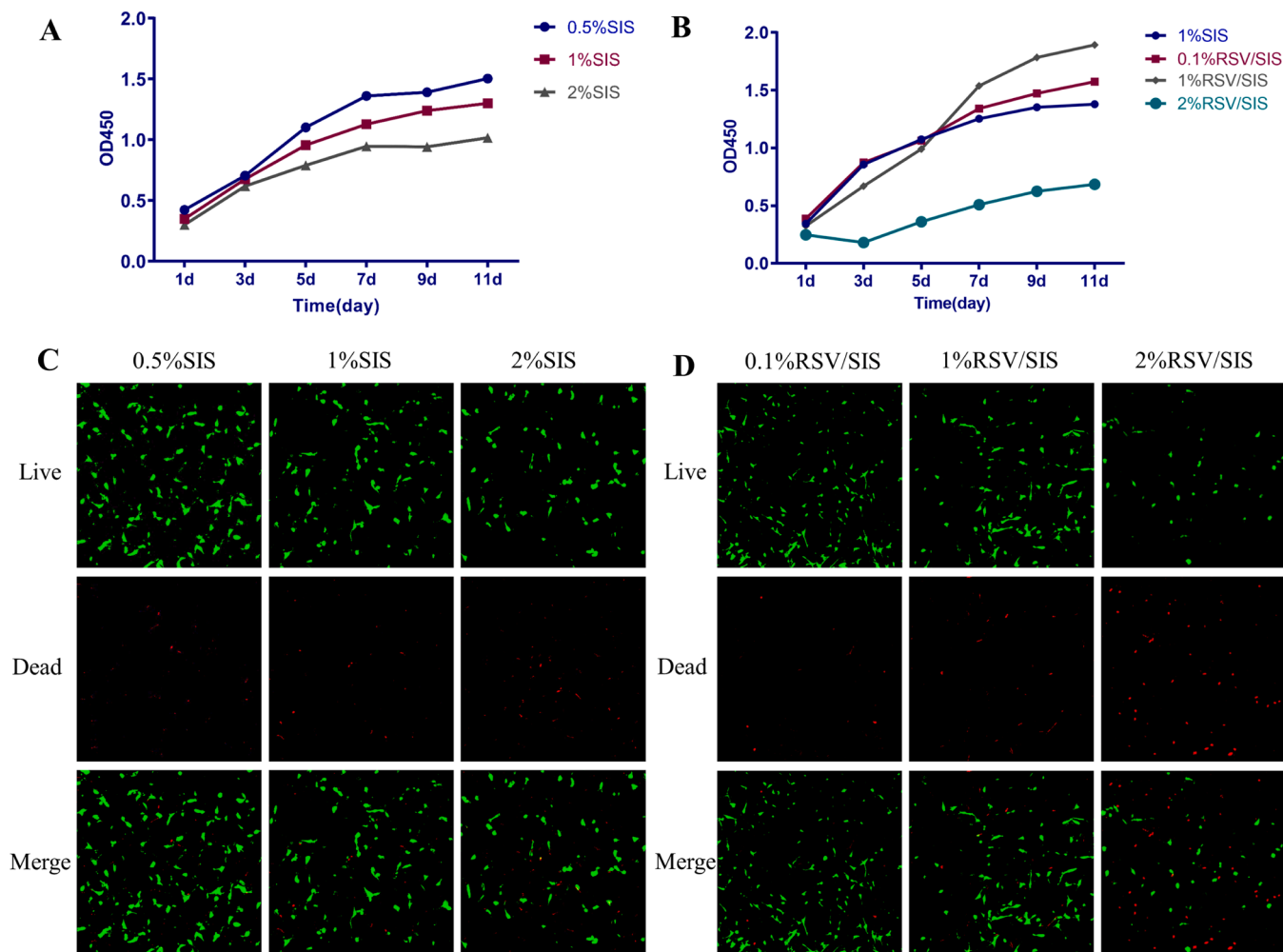


Fig. 3. *In vitro* biocompatibility of the SIS and RSV/SIS scaffolds. Cell proliferation of hBMSCs on (A) SIS scaffolds and (B) RSV/SIS scaffolds. Cell viability of hBMSCs on (C) SIS scaffolds and (D) RSV/SIS scaffolds.

divided into three groups ($n = 4$) based on the type of defect: defect only (blank control group), defect plus implantation of 1% SIS scaffolds (1% SIS group), and defect plus implantation of 1% RSV/SIS scaffolds (1% RSV/SIS group). Then, the incisions were sutured hierarchically.

The rats were euthanized at 4 weeks after the surgery. The excised calvarias were fixed with 4% paraformaldehyde for 24 h. After paraffin sectioning, the samples were stained with haematoxylin and eosin (HE) and Masson's trichrome and used for histological observation. To analyse the expression of RUNX2 and CD31 in the bone defect area, paraffin sections were also stained for immunohistochemical analysis. Image J software (Media Cybernetic, USA) was used to conduct quantitative analysis.

2.4. Statistical analysis

Statistical analysis was performed using SPSS 23.0 software (IBM, USA). The data are expressed as the mean \pm standard deviation. Independent sample t-tests were used to compare the means between two groups. One-way analysis of variance followed by Tukey's or Dunnett's *post hoc* test and Fisher's least significant difference test was used to compare more than two groups. $P < 0.05$ was considered to indicate statistical significance.

3. Results and discussion

3.1. Characterization of SIS scaffolds

3.1.1. Morphological observations

Fig. 1A presents ESEM micrographs of the internal structure of the SIS scaffolds prepared with different concentrations of SIS. All of the samples had a highly porous sponge-like structure with interconnected and regular pores. As the SIS concentration increased, the structure of the SIS scaffolds gradually became more compact.

3.1.2. Pore size

The average pore sizes (Fig. 2B) of the 0.5% SIS and 1% SIS scaffolds were $257.645 \pm 78.799 \mu\text{m}$ and $191.036 \pm 33.853 \mu\text{m}$, respectively, which are suitable for bone regeneration [40,41]. Macroporous scaffolds can be more easily integrated with host bone tissue, thus facilitating angiogenesis and bone ingrowth [1]. The mean pore size of the 2% SIS scaffolds was significantly smaller than those of the other two groups ($P < 0.05$).

3.1.3. Porosity

The porosity test (Fig. 2C) revealed significant differences among the three groups ($P < 0.05$). Among them, the porosity of the 0.5% SIS and 1% SIS scaffolds reached more than 80%, which has been confirmed to be very important for the migration and proliferation of osteoblasts and mesenchymal cells, as well as vascularization [19].

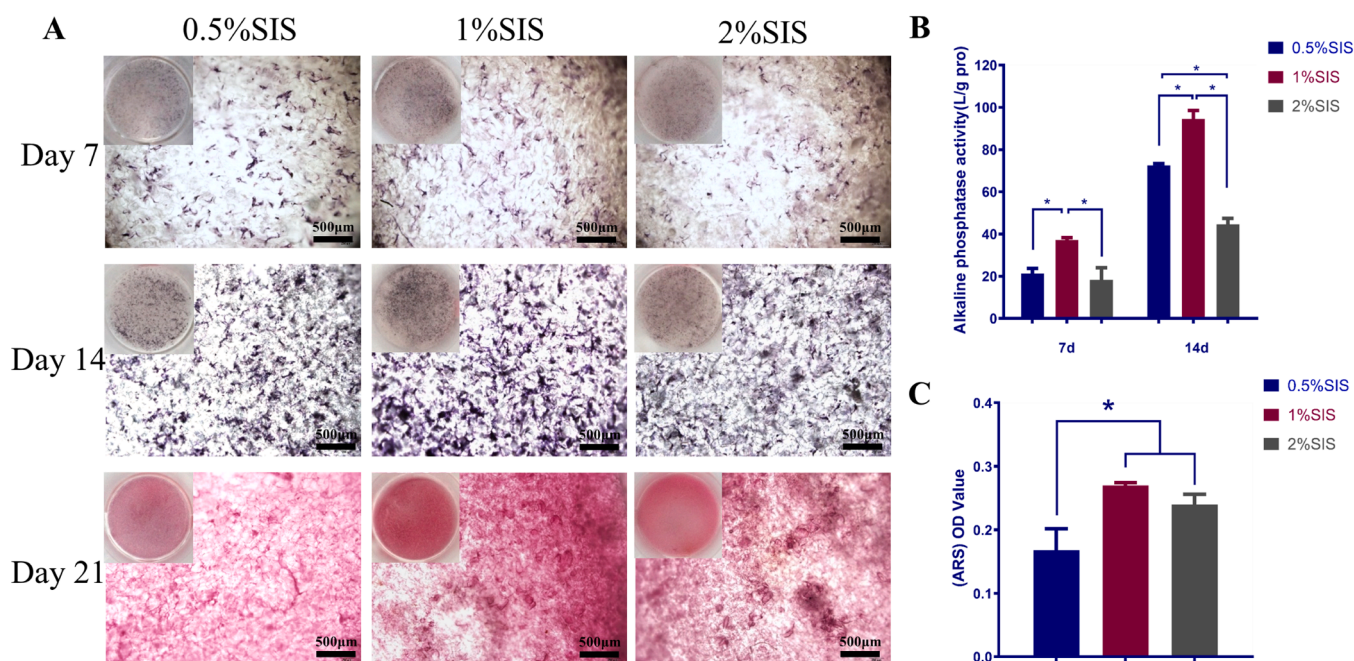


Fig. 4. ALP and ARS staining and quantitation of hBMSCs on SIS scaffolds (A) ALP and ARS staining. (B) ALP activities. (C) Quantitative analysis of ARS staining. *, $P < 0.05$.

3.1.4. In vitro degradation

The degradation of the scaffolds was expressed as the degradation percentage over time. As shown in Fig. 2D, the degradation rate of the 0.5%SIS, 1%SIS and 2%SIS scaffolds was approximately 100%, 63% and 55%, respectively, after 28 days. The degradation rate appeared to be higher for the 0.5%SIS scaffolds than for the other two scaffold types. This may be attributable to the higher specific surface area of this type of scaffold due to its large pore size and high porosity [42].

3.2. Characterization of RSV/SIS scaffolds

3.2.1. Morphological and structure observations

Similar to the pure SIS scaffolds, the microstructure of the RSV/SIS scaffolds (Fig. 2A) maintained pores of a uniform shape. The average pore size of the 1%RSV/SIS scaffold was $171.959 \pm 29.937 \mu\text{m}$, which was smaller than that of the 1%SIS scaffold ($191.036 \pm 33.853 \mu\text{m}$). However, this difference was not statistically significant ($P < 0.05$), indicating that RSV functionalization did not markedly affect the structure of the SIS scaffolds.

The FTIR spectra of the RSV, SIS scaffolds and RSV/SIS scaffolds are displayed in Fig. 2B. For RSV, the absorption peak at 1153 cm^{-1} was the stretching vibration of C-OH; 831 cm^{-1} was the characteristic absorption peak of the out-of-plane bending vibration of C-H on the benzene ring. Compared with the 1%SIS scaffolds, new absorption peaks were generated at 1162 cm^{-1} and 844 cm^{-1} in the infrared spectrum of the 1% RSV/SIS scaffolds, due to the C-OH and benzene ring C-H in RSV. This indicates that RSV was effectively immobilized on the SIS scaffolds by forming covalent bond.

3.2.2. Drug loading and in vitro drug release

The effects of different RSV concentrations on drug loading of the 1% SIS scaffolds were examined via ultraviolet spectrophotometry. The results (Fig. 2C) showed that the concentration of RSV used for coupling was proportional to drug loading onto the scaffolds. We then evaluated the cumulative release of RSV from the RSV/SIS scaffolds. As shown in Fig. 2D, RSV release was closely related with the amount of drug loaded onto the scaffolds. All scaffolds released an initial burst of RSV within the first day, which might have been caused by the dissolution of drug

molecules deposited on the surface of the samples [43]. From the next day, the release rate gradually slowed and plateaued within 1 week. Following this, the release was slow and steady for at least 21 days, indicating that RSV was effectively immobilized on the SIS scaffolds. This sustained slow RSV release could be attributed to the covalent coupling of the SIS carboxylic acid moiety with the hydroxyl group in RSV to form an ester bond with EDC as a coupling agent [34]. It could also be attributed to the low solubility of RSV in water, such that the conjugate formed from ester bonding between RSV and SIS could only be slowly hydrolysed [35].

3.3. In vitro biocompatibility

Biocompatibility is the most important factor in the design of scaffolds. We used CCK-8 and live/dead assays to explore the proliferation and viability of hBMSCs on different scaffolds. Specifically, we wanted to clarify the effects of pore structure and RSV functionalization on the biocompatibility of the scaffolds.

For all three groups of SIS scaffolds, the results of CCK-8 assays (Fig. 3A) showed that the OD values of all samples gradually increased over time. This indicates that the SIS scaffolds exhibited good biocompatibility, consistent with previous studies [15,44]. In the scaffolds with larger pores, a greater number of cells was found. This indicates that pore structure had certain effects on cell proliferation. Fluorescent images were obtained at 1 day after cell seeding. As shown in Fig. 3C, cell seeding resulted in a regular dispersion of cells on all samples. Consistent with the CCK-8 results, most of the cells were viable (stained green), with relatively few dead cells (stained red) found, and the cell activity on the 0.5%SIS scaffold was the highest among the three groups. This further confirmed the good biocompatibility of the SIS scaffolds, as well as indicates that the macroporous scaffold was more conducive to cell viability. However, in previous studies, the effect of pore structure on cell proliferation and viability on a scaffold is non-linear. Specifically, smaller pores have a larger specific surface area, which facilitates initial cell adhesion, whereas larger pores provide more space, which allows improved cell infiltration [40].

The results of the CCK-8 assays analysing the drug loading on the three RSV/SIS scaffolds are shown in Fig. 3B. Cell proliferation on the

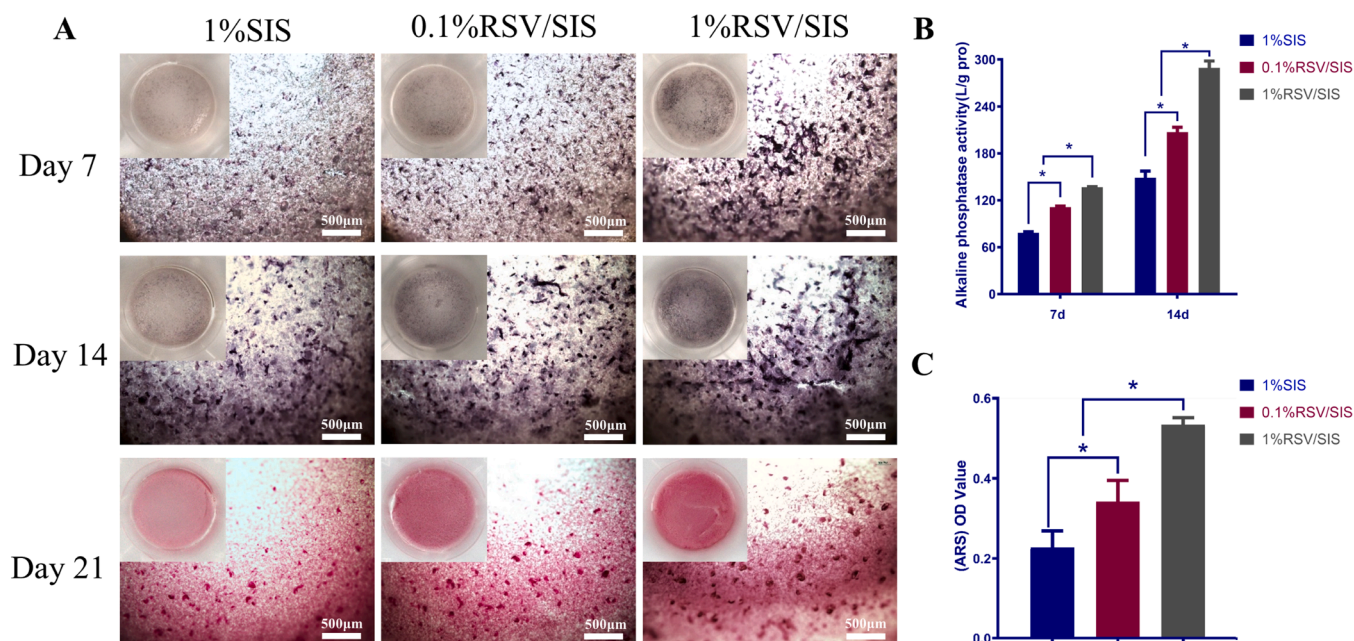


Fig. 5. ALP and ARS staining and quantitation of hBMSCs on RSV/SIS scaffolds. (A) ALP and ARS staining. (B) ALP activity. (C) Quantitative analysis of ARS staining. *, $P < 0.05$.

0.1%RSV/SIS and 1%RSV/SIS scaffolds and the blank SIS scaffolds was significantly better than that on the 2%RSV/SIS scaffolds. Similarly, the live/dead assays showed that the number of dead cells on the 2%RSV/SIS scaffolds was significantly higher than those in the other groups (Fig. 3D). Accordingly, this group was excluded from subsequent analyses. These data revealed that RSV incorporation may have a dose-dependent effect on cell proliferation and viability [45]. The high concentration of RSV might have exerted an inhibitory effect on hBMSCs, which is in accordance with previous studies [46]. Further, the OD values of the 1%RSV/SIS scaffolds were slightly lower in the first 3 days after cell seeding. This might have been due to the burst release of drug from the scaffolds at the initial stage, resulting in a temporarily high concentration of RSV. Accordingly, the proliferation of hBMSCs might have been promoted at lower RSV concentrations at the later stage [46].

3.4. *In vitro* osteogenic differentiation

BMSCs undergo three different growth processes: proliferation, maturation and mineralization. The key evidence for BMSC differentiation is the identification of osteogenic markers in *in vitro* cell culture [27]. In addition, the expression of various marker genes at the early, middle and late stages of cell differentiation is important in clarifying the effect of scaffold type on the osteogenic differentiation activity of BMSCs [27].

3.4.1. ALP and ARS staining and quantitation

ALP activity and calcified nodules present after mineralization are two markers that are commonly used to detect the early and late differentiation of BMSCs [47]. Fig. 4 shows the effects of pore structure on ALP expression and the mineralization of hBMSCs cultured on the SIS scaffolds. The ALP staining and quantitative activity data (Fig. 4A, B) showed that ALP expression on the 1%SIS scaffolds was significantly higher than that in the other two groups ($P < 0.05$) at both 7 and 14 days after osteogenic induction. ARS staining and quantitative analysis (Fig. 4A, C) showed the same trend on day 21. The number of calcified nodules on the 1%SIS scaffolds was significantly higher than that on the 0.5%SIS scaffolds ($P < 0.05$) and slightly greater than that on the 2%SIS scaffolds, although the latter difference was not significant ($P > 0.05$). Further, ALP expression in the 0.5%SIS scaffold group was significantly

higher than that in the 2%SIS scaffold group on day 14 ($P < 0.05$). Mineralization on day 21 was significantly worse in the 0.5%SIS scaffold group than the other two groups ($P < 0.05$), which might have been due to the above-mentioned increase in degradation rate that likely resulted in the loss of structural integrity and functionality [48]. In general, our results indicate that pore structure can affect osteogenesis on the SIS scaffolds. Among the three groups, the 1%SIS scaffolds had the most favourable pore structure for osteogenic differentiation of hBMSCs. Therefore, we conducted follow-up studies of RSV functionalization using the 1%SIS scaffolds.

We explored the effects of RSV functionalization on the osteogenic properties of SIS scaffolds *in vitro*. As shown in Fig. 5A, the staining results showed that the signals associated with ALP and calcium nodules for cells inoculated on the two types of RSV/SIS scaffolds were much stronger than those for the SIS scaffolds in the blank control group. Consistent with the staining results, quantitative analysis (Fig. 5B, C) showed that ALP activity and calcium accumulation rates were significantly higher for the two types of RSV/SIS scaffolds compared with the SIS scaffolds ($P < 0.05$), which indicates that RSV functionalization notably enhanced the osteogenic ability of the SIS scaffolds. Enhanced osteogenic activity was observed by Pandelet et al., who covalently immobilized RSV on cellulose acetate membranes, and Cai et al., who incorporated RSV into PEEK/nMCS composites [33,34]. In the present study, the 1%RSV/SIS scaffolds with higher drug loading also exhibited higher ALP activity and greater calcium deposit accumulation compared with the 0.1%RSV/SIS scaffolds. This indicates that the promotional effects were related to the RSV concentration, which is consistent with previous studies reporting that the promotion of osteogenic differentiation was dose-dependent [49].

3.4.2. Bone-related gene expression

Based on the above evidence, the two groups of the 2%SIS scaffolds and the 0.1%RSV/SIS scaffolds were excluded from subsequent experiments. To further clarify the effects of pore structure and RSV functionalization on the expression of osteogenesis-related genes on the SIS scaffolds, we subjected the 0.5%SIS, 1%SIS, and 1%RSV/SIS scaffolds to a real-time qPCR assay and conducted pairwise comparisons. As shown in Fig. 6, we evaluated the expression of early-stage osteoblast differentiation markers (RUNX2, COL-1 and BMP-2), middle-stage markers

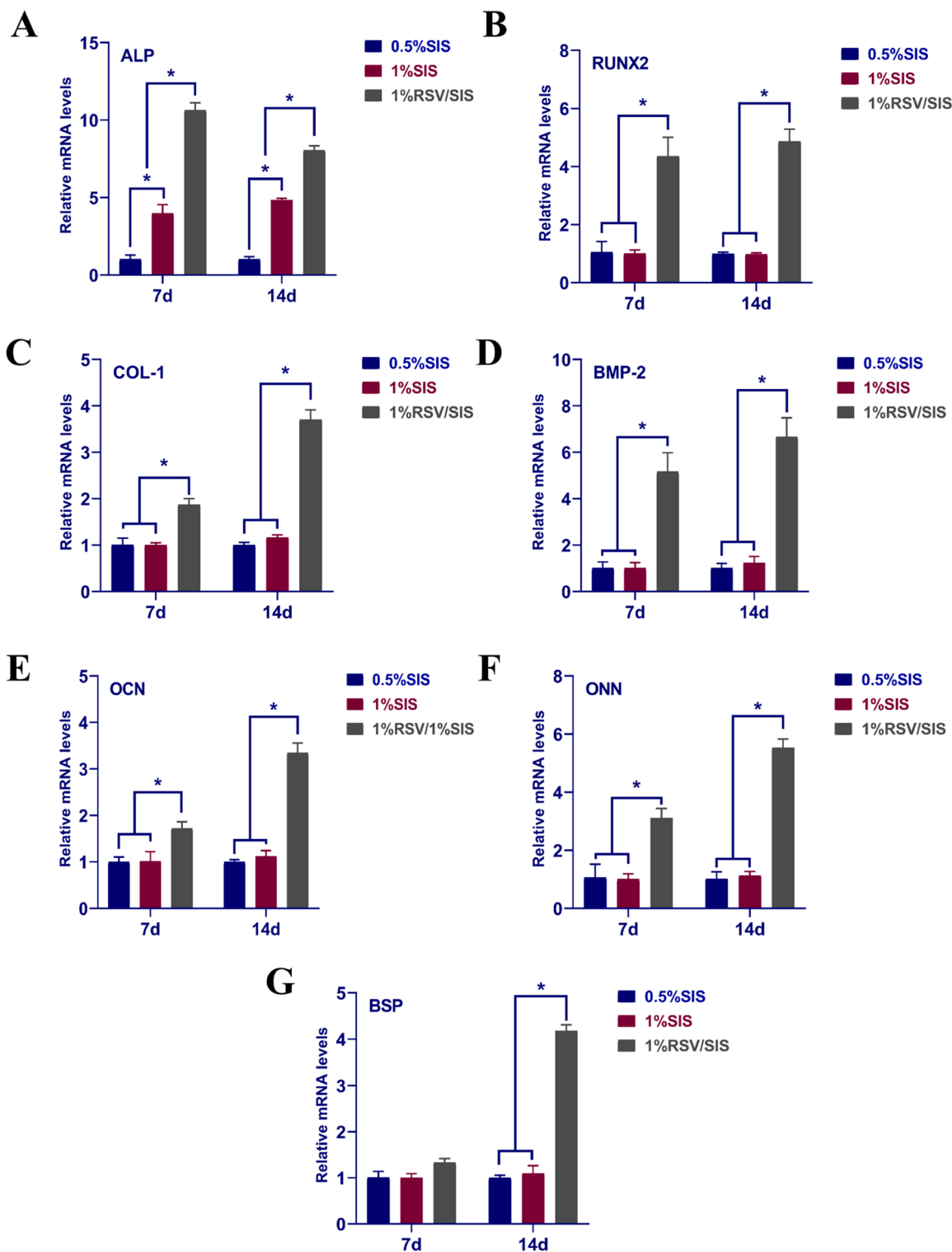


Fig. 6. Relative mRNA expression levels of (A) ALP, (B) RUNX2, (C) COL-1, (D) BMP-2, (E) OCN, (F) ONN and (G) BSP on days 7 and 14 after *in vitro* osteogenic induction of hBMSCs. *, $P < 0.05$.

(ALP) and late-stage markers (OCN, ONN and BSP).

Comparing the 0.5%SIS scaffolds and 1%SIS scaffolds, we found significant differences in ALP expression at the two time points tested ($P < 0.05$). However, we found no significant differences for the other five genes ($P > 0.05$), indicating that the pore structure only affected the expression of the early marker ALP. The enhanced osteogenic differentiation of hBMSCs on the 1%SIS scaffold despite the relatively small pore

structure may be related to how mechanical stimulation affects cell differentiation [50]. On scaffolds with relatively large pores, most cells can only attach to a single pillar to experience mechanical stimulation. By contrast, on scaffolds with small pores, cells can spread to several pillars and are more likely to receive mechanical stimulation, leading to a greater chance of differentiation [51].

We compared the 1%SIS scaffolds and 1%RSV/SIS scaffolds to

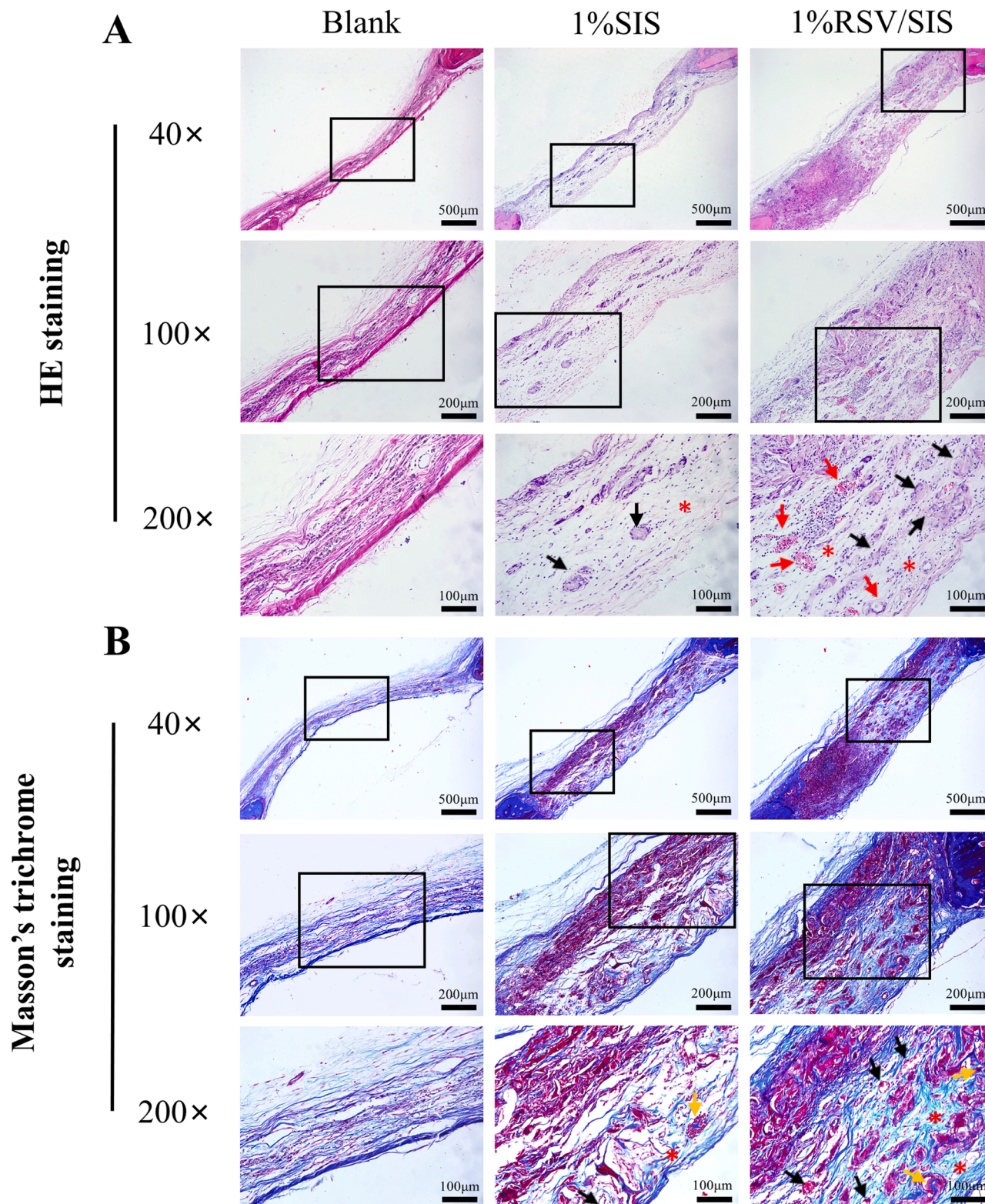


Fig. 7. Bone regeneration in critical-size calvarial defects. (A) HE staining. Red asterisk: residual scaffolds; black arrow: new bone; red arrow: blood vessel. (B) Masson's trichrome staining. Red asterisk: residual scaffolds; yellow arrow: new bone; black arrow: blood vessel.

determine whether the released RSV could orchestrate osteoblast differentiation. As shown in Fig. 6, RSV functionalization significantly upregulated the expression of all genes tested ($P < 0.05$). Additionally, RSV can enhance calcium deposition and accelerate bone mineralization [52]. We speculate that the release of RSV might have enhanced osteogenic differentiation, which might in turn accelerate bone

mineralization through enhanced calcium deposition [53,54]. RSV was previously reported to increase ALP activity via SIRT1 activation of BMP2, thus inducing osteoblastic differentiation and promoting the mineralization of BMSCs [55]. As a potential underlying mechanism, RSV may activate the Wnt/ β -catenin signalling pathway to increase the expression of bone formation markers. However, this requires further

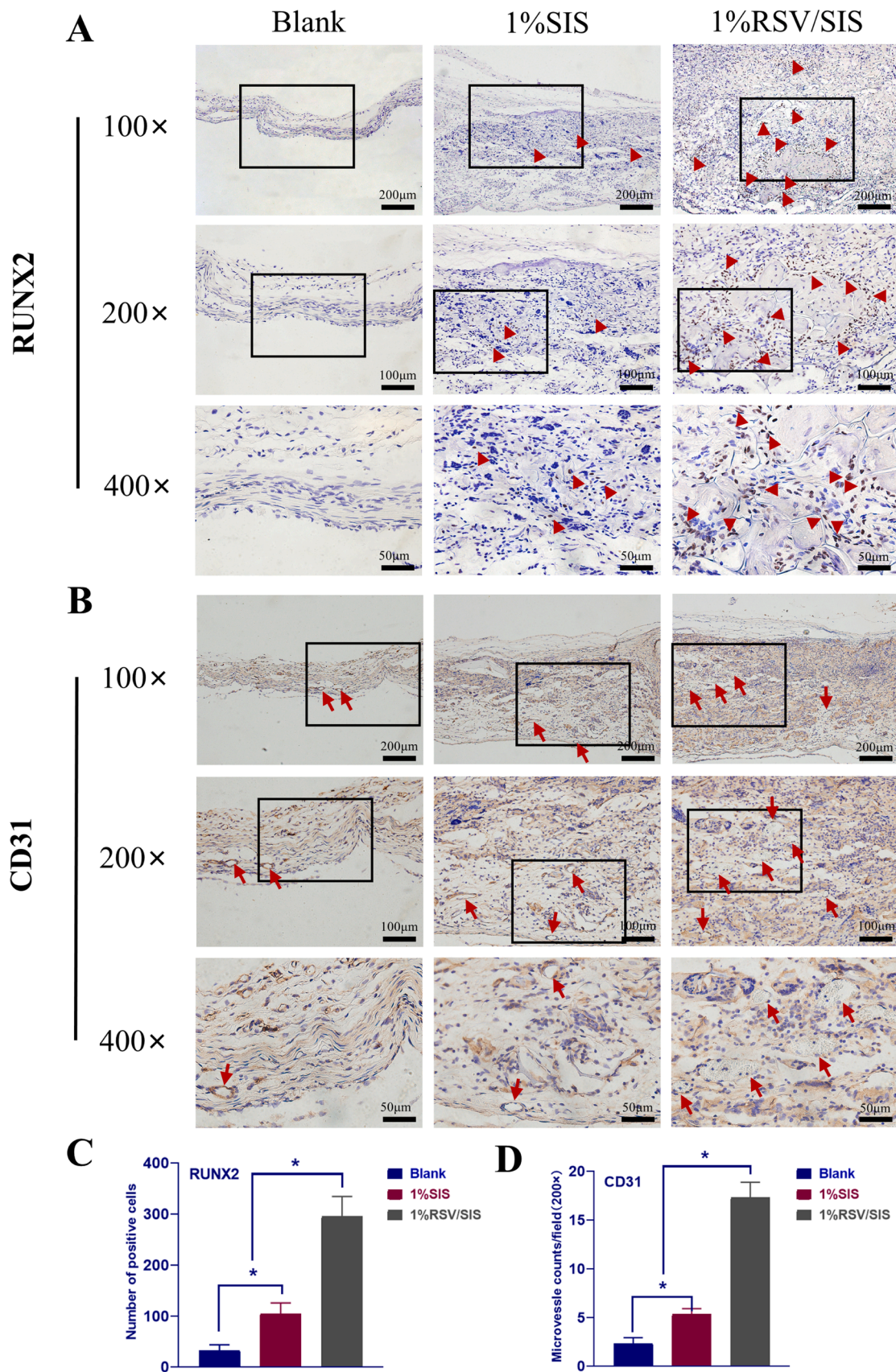


Fig. 8. Bone regeneration in critical-size calvarial defects. (A, C) Immunohistochemical staining and quantitative analysis of RUNX2. Red triangle: RUNX2-labelled cells. (B, D) Immunohistochemical staining and quantitative analysis of CD31. Red arrow: CD31-labelled blood vessels. *, $P < 0.05$.

investigation.

3.5. *In vivo* bone formation

We explored the effects of structural optimization and RSV functionalization on the osteogenic properties of SIS scaffolds *in vivo* using an early healing rat model of critical bone defects.

HE staining (Fig. 7A) showed that in the blank control group, the bone defects were filled with thin and loose fibrous connective tissue at 4 weeks after the operation, and no obvious new bone formation was observed. This indicated that the circular full-thickness bone defect with a diameter of 5 mm met the critical-size standard [56]. In the 1%SIS group, a small amount of new osteoid tissue was distributed in a scattered manner, and some osteoblasts and new blood vessels could be seen. This indicated that implantation of the 1%SIS scaffolds facilitated bone defect healing. In the 1%RSV/SIS group, we detected a large number of new bone matrices scattered in the bone defect area. These were surrounded by a dense array of osteoblasts as well as new blood vessels. The results of Masson's trichrome staining (Fig. 7B) were basically consistent with the results of HE staining. Specifically, compared with the blank control group, more new bone formation took place in the 1%SIS group and 1%RSV/SIS group, especially in the latter group. This suggests that RSV functionalization can improve the osteogenic activity of SIS scaffolds *in vivo*. Previous studies have reported similar findings. For example, Wang et al. found that collagen scaffolds loaded with RSV could promote bone regeneration more effectively than simple collagen scaffolds [57]. Further, Lu et al. found that RSV could promote the migration of endothelial progenitor cells and angiogenesis [58].

Immunohistochemical staining and quantitative analysis (Fig. 8) further confirmed the osteoblast aggregation and more blood vessel formation observed with HE and Masson's trichrome staining. Compared with the blank control group, the 1%SIS group exhibited greater expression of RUNX2 (osteogenic marker protein). Moreover, there appeared to be a broader distribution and significantly higher proportion of RUNX2 in the 1%RSV/SIS group than in the 1%SIS group ($P < 0.05$), which was consistent with our observation that RSV functionalization significantly upregulated the gene expression of RUNX2 on SIS scaffolds *in vitro*. In addition, the expression of CD31 (angiogenic protein marker) in the 1%RSV/SIS group was significantly higher than that in the other two groups ($P < 0.05$). This explained the phenomenon of more neovascularization, which is closely related to the transport of nutrients and mineralization-related substances such as calcium and phosphorus, as well as the recruitment of osteoblast-related cells [59, 60]. However, whether the RSV/SIS scaffolds is conducive to early vascularization still needs to more evidence. Besides, animal studies with larger sample sizes and longer observation periods are necessary to further explore the *in vivo* osteogenic potential of the RSV/SIS scaffolds.

4. Conclusion

Pore structure and RSV functionalization significantly improved the osteogenic activity of SIS scaffolds. SIS scaffolds with a fabrication concentration of 1% had superior osteogenic properties. Through covalent coupling, RSV was successfully grafted onto SIS scaffolds, where it was slowly released. The most significant improvements in osteogenic properties were obtained with a coupling concentration of 1%. In *in vivo* experiments, vascular and new bone formation were enhanced with RSV/SIS scaffolds compared with either SIS scaffolds or the blank control group at 4 weeks after implantation. These findings demonstrate the promise of RSV/SIS scaffolds obtained via dual optimization strategies as biomaterials in bone tissue engineering.

CRediT authorship contribution statement

Bowen Li: Methodology, Validation, Formal analysis, Resources, Writing – original draft. **Mei Wang:** Investigation, Data curation. **Yuhua**

Liu: Conceptualization, Supervision, Writing – review & editing. **Yongsheng Zhou:** Supervision, Writing – review & editing. **Lin Tang:** Investigation, Formal analysis. **Pengyue You:** Investigation. **Yi Deng:** Investigation.

Declaration of Competing Interest

The authors declare that they have no known competing financial interests or personal relationships that could have appeared to influence the work reported in this paper.

References

- [1] A.H. Reddi, Morphogenesis and tissue engineering of bone and cartilage: inductive signals, stem cells, and biomimetic biomaterials, *Tissue Eng.* 6 (4) (2000) 351–359.
- [2] S. Cao, Y. Zhao, Y. Hu, L. Zou, J. Chen, New perspectives: in-situ tissue engineering for bone repair scaffold, *Compos. Part B: Eng.* 202 (2020), 108445.
- [3] L. Li, H. Lu, Y. Zhao, J. Luo, L. Yang, W. Liu, Q. He, Functionalized cell-free scaffolds for bone defect repair inspired by self-healing of bone fractures: a review and new perspectives, *Mater. Sci. Eng.: C* 98 (2019) 1241–1251.
- [4] T. Xu, Q. Yao, J.M. Miszuk, H.J. Sanyour, Z. Hong, H. Sun, H. Fong, Tailoring weight ratio of PCL/PLA in electrospun three-dimensional nanofibrous scaffolds and the effect on osteogenic differentiation of stem cells, *Colloids Surf. B: Biointerfaces* 171 (2018) 31–39.
- [5] W. Li, H. Xu, X. Han, S. Sun, Q. Chai, X. Xu, Z. Man, Simultaneously promoting adhesion and osteogenic differentiation of bone marrow-derived mesenchymal cells by a functional electrospun scaffold, *Colloids Surf. B: Biointerfaces* 192 (2020), 111040.
- [6] C. Qi, Y. Deng, L. Xu, C. Yang, Y. Zhu, G. Wang, Z. Wang, L. Wang, A sericin/graphene oxide composite scaffold as a biomimetic extracellular matrix for structural and functional repair of calvarial bone, *Theranostics* 10 (2) (2020) 741–756.
- [7] J. He, G. Chen, M. Liu, Z. Xu, H. Chen, L. Yang, Y. Lv, Scaffold strategies for modulating immune microenvironment during bone regeneration, *Mater. Sci. Eng. C Mater. Biol. Appl.* 108 (2020), 110411.
- [8] J. De Waele, K. Reekmans, J. Daans, H. Goossens, Z. Berneman, P. Ponsaerts, 3D culture of murine neural stem cells on decellularized mouse brain sections, *Biomaterials* 41 (2015) 122–131.
- [9] V. Navarro-Tableros, M.B. Herrera Sanchez, F. Figliolini, R. Romagnoli, C. Tetta, G. Camussi, Recellularization of rat liver scaffolds by human liver stem cells, *Tissue Eng. - Part A* 21 (11–12) (2015) 1929–1939.
- [10] D.A. Taylor, L.C. Sampaio, Z. Ferdous, A.S. Gobin, L.J. Taite, Decellularized matrices in regenerative medicine, *Acta Biomater.* 74 (2018) 74–89.
- [11] Q. Yao, Y.-W. Zheng, Q.-H. Lan, L. Kou, H.-L. Xu, Y.-Z. Zhao, Recent development and biomedical applications of decellularized extracellular matrix biomaterials, *Mater. Sci. Eng.: C* 104 (2019), 109942.
- [12] H. Xing, H. Lee, L. Luo, T.R. Kyriakides, Extracellular matrix-derived biomaterials in engineering cell function, *Biotechnol. Adv.* 42 (2020), 107421.
- [13] Y. Ji, J. Zhou, T. Sun, K. Tang, Z. Xiong, Z. Ren, S. Yao, K. Chen, F. Yang, F. Zhu, X. Guo, Diverse preparation methods for small intestinal submucosa (SIS): decellularization, components, and structure, *J. Biomed. Mater. Res. Part A* 107 (3) (2019) 689–697.
- [14] J.-C. Luo, W. Chen, X.-H. Chen, T.-W. Qin, Y.-C. Huang, H.-Q. Xie, X.-Q. Li, Z.-Y. Qian, Z.-M. Yang, A multi-step method for preparation of porcine small intestinal submucosa (SIS), *Biomaterials* 32 (3) (2011) 706–713.
- [15] M. Li, C. Zhang, M. Cheng, Q. Gu, J. Zhao, Small intestinal submucosa: a potential osteoconductive and osteoinductive biomaterial for bone tissue engineering, *Mater. Sci. Eng.: C* 75 (2017) 149–156.
- [16] K.S. Kim, J.Y. Lee, Y.M. Kang, E.S. Kim, G.H. Kim, S.D. Rhee, H.G. Cheon, J.H. Kim, B.-H. Min, H.B. Lee, M.S. Kim, Small intestine submucosa sponge for *in vivo* support of tissue-engineered bone formation in the presence of rat bone marrow stem cells, *Biomaterials* 31 (6) (2010) 1104–1113.
- [17] S.G. Caridade, J.F. Mano, Engineering membranes for bone regeneration, *Tissue Eng. Part A* 23 (23–24) (2017) 152–1533.
- [18] L. Rosefi, V. Parisi, M. Petretta, C. Cavallo, G. Desando, I. Bartolotti, B. Grigolo, Scaffolds for bone tissue engineering: state of the art and new perspectives, *Mater. Sci. Eng.: C* 78 (2017) 1246–1262.
- [19] V. Karageorgiou, D. Kaplan, Porosity of 3D biomaterial scaffolds and osteogenesis, *Biomaterials* 26 (27) (2005) 5474–5491.
- [20] C.M. Murphy, F.J. O'Brien, Understanding the effect of mean pore size on cell activity in collagen-glycosaminoglycan scaffolds, *Cell Adhes. Migr.* 4 (3) (2010) 377–381.
- [21] N. Abbasi, A. Abdal-hay, S. Hamlet, E. Graham, S. Ivanovskii, Effects of gradient and offset architectures on the mechanical and biological properties of 3-D melt electrowritten (MEW) scaffolds, *ACS Biomater. Sci. Eng.* 5 (7) (2019) 3448–3461.
- [22] A. Bignon, J. Chouteau, J. Chevalier, G. Fantozzi, J.P. Carret, P. Chavassieux, G. Boivin, M. Melin, D. Hartmann, Effect of micro- and macroporosity of bone substitutes on their mechanical properties and cellular response, *J. Mater. Sci. Mater. Med.* 14 (12) (2003) 1089–1097.
- [23] B. Zhang, H. Li, L. He, Z. Han, T. Zhou, W. Zhi, X. Lu, X. Lu, J. Weng, Surface-decorated hydroxyapatite scaffold with on-demand delivery of dexamethasone and

- stromal cell derived factor-1 for enhanced osteogenesis, *Mater. Sci. Eng.: C* 89 (2018) 355–370.
- [24] W. Shi, M. Sun, X. Hu, B. Ren, J. Cheng, C. Li, X. Duan, X. Fu, J. Zhang, H. Chen, Y. Ao, Structurally and functionally optimized silk-fibroin-gelatin scaffold using 3D printing to repair cartilage injury in vitro and in vivo, *Adv. Mater.* 29 (29) (2017), 1701089.
- [25] L. Sun, C.B. Danoux, Q. Wang, D. Pereira, D. Barata, J. Zhang, V. LaPointe, R. Truckenmüller, C. Bao, X. Xu, P. Habibovic, Independent effects of the chemical and microstructural surface properties of polymer/ceramic composites on proliferation and osteogenic differentiation of human MSCs, *Acta Biomater.* 42 (2016) 364–377.
- [26] I.M. Wojak-Ćwik, Ł. Rumian, M. Krok-Borkowicz, R. Hess, R. Bernhardt, P. Dobrzyński, S. Möller, M. Schnabelrauch, V. Hintze, D. Scharnweber, E. Pamula, Synergistic effect of bimodal pore distribution and artificial extracellular matrices in polymeric scaffolds on osteogenic differentiation of human mesenchymal stem cells, *Mater. Sci. Eng.: C* 97 (2019) 12–22.
- [27] K.T. Shalumon, H.-T. Liao, C.-Y. Kuo, C.-B. Wong, C.-J. Li, M. P.A. J.-P. Chen, Rational design of gelatin/nanohydroxyapatite cryogel scaffolds for bone regeneration by introducing chemical and physical cues to enhance osteogenesis of bone marrow mesenchymal stem cells, *Mater. Sci. Eng.: C* 104 (2019), 109855.
- [28] S. Bagherifard, Mediating bone regeneration by means of drug eluting implants: from passive to smart strategies, *Mater. Sci. Eng.: C* 71 (2017) 1241–1252.
- [29] M.A. Fernandez-Yague, S.A. Abbah, L. McNamara, D.I. Zeugolis, A. Pandit, M. J. Biggs, Biomimetic approaches in bone tissue engineering: integrating biological and physicochemical strategies, *Adv. Drug Deliv. Rev.* 84 (2015) 1–29.
- [30] D. Murgia, R. Mauceci, G. Campisi, V. De Caro, Advance on resveratrol application in bone regeneration: progress and perspectives for use in oral and maxillofacial surgery, *Biomolecules* 9 (3) (2019) 94.
- [31] V. Martin, A. Bettencourt, Bone regeneration: biomaterials as local delivery systems with improved osteoinductive properties, *Mater. Sci. Eng. C Mater. Biol. Appl.* 82 (2018) 363–371.
- [32] M.S. Kamath, S.S.S.J. Ahmed, M. Dhanasekaran, S.W. Santosh, Polycaprolactone scaffold engineered for sustained release of resveratrol: therapeutic enhancement in bone tissue engineering, *Int. J. Nanomed.* 9 (2014) 183–195.
- [33] G. Cai, H. Wang, Y.K. Jung, Z. Xu, J. Zhang, J. He, D. Wang, J.-W. Shin, R. Kaewmanee, S. Nabanita, J. Wei, Hierarchically porous surface of PEEK/nMCS composite created by femtosecond laser and incorporation of resveratrol exhibiting antibacterial performances and osteogenic activity in vitro, *Compos. Part B: Eng.* 186 (2020), 107802.
- [34] A.M. Pandeale, P. Neacsu, A. Cimpean, A.I. Staras, F. Miculescu, A. Iordache, S. I. Voicu, V.K. Thakur, O.D. Toader, Cellulose acetate membranes functionalized with resveratrol by covalent immobilization for improved osseointegration, *Appl. Surf. Sci.* 438 (2018) 2–13.
- [35] Y. Li, S. Dänmark, U. Edlund, A. Finne-Wistrand, X. He, M. Norgård, E. Blomén, K. Hultenby, G. Andersson, U. Lindgren, Resveratrol-conjugated poly-ε-caprolactone facilitates in vitro mineralization and in vivo bone regeneration, *Acta Biomater.* 7 (2) (2011) 751–758.
- [36] H.-T. Lu, T.-W. Lu, C.-H. Chen, F.-L. Mi, Development of genipin-crosslinked and fucoidan-adsorbed nano-hydroxyapatite/hydroxypropyl chitosan composite scaffolds for bone tissue engineering, *Int. J. Biol. Macromol.* 128 (2019) 973–984.
- [37] H.X. Wang, Z.Y. Li, Z.K. Guo, Z.K. Guo, Easily-handled method to isolate mesenchymal stem cells from coagulated human bone marrow samples, *World J. Stem Cells* 7 (8) (2015) 1137–1144.
- [38] Y. Huang, D. Seitz, F. König, P.E. Müller, V. Jansson, R.M. Klar, Induction of articular chondrogenesis by chitosan/hyaluronic-acid-based biomimetic matrices using human adipose-derived stem cells, *Int. J. Mol. Sci.* 20 (18) (2019) 4487.
- [39] K.J. Livak, T.D. Schmittgen, Analysis of relative gene expression data using real-time quantitative PCR and the 2^{-ΔΔCT} method, *Methods* 25 (4) (2001) 402–408.
- [40] S.W. Choi, Y. Zhang, Y. Xia, Three-dimensional scaffolds for tissue engineering: the importance of uniformity in pore size and structure, *Langmuir: ACS J. Surf. Colloids* 26 (24) (2010) 19001–19006.
- [41] N. Abbasi, S. Hamlet, R.M. Love, N.-T. Nguyen, Porous scaffolds for bone regeneration, *J. Sci.: Adv. Mater. Devices* 5 (1) (2020) 1–9.
- [42] Y.C. Lin, F.J. Tan, K.G. Marra, S.S. Jan, D.C. Liu, Synthesis and characterization of collagen/hyaluronan/chitosan composite sponges for potential biomedical applications, *Acta Biomater.* 5 (7) (2009) 2591–2600.
- [43] V. Pawar, U. Bulbake, W. Khan, R. Srivastava, Chitosan sponges as a sustained release carrier system for the prophylaxis of orthopedic implant-associated infections, *Int. J. Biol. Macromol.* 134 (2019) 100–112.
- [44] H. Li, T. Ji, L.Q. Xu, Y.J. Hu, S.Y. Li, C.P. Zhang, Study on the osteogenesis ability of co-culturing bone marrow stromal cells (BMSCs) and small intestinal submucosa, *Shanghai kou qiang yi xue = Shanghai J. Stomatol.* 15 (2) (2006) 167–171.
- [45] Z. Safaeinejad, F. Kazeminasab, A. Kiani-Esfahani, K. Ghaedi, M.H. Nasr-Esfahani, Multi-effects of Resveratrol on stem cell characteristics: Effective dose, time, cell culture conditions and cell type-specific responses of stem cells to Resveratrol, *Eur. J. Med. Chem.* 155 (2018) 651–657.
- [46] T. Zhou, Y. Yan, C. Zhao, Y. Xu, Q. Wang, N. Xu, Resveratrol improves osteogenic differentiation of senescent bone mesenchymal stem cells through inhibiting endogenous reactive oxygen species production via AMPK activation, *Redox Rep.* 24 (1) (2019) 62–69.
- [47] Y. Yu, Y. Sun, X. Zhou, Y. Mao, Y. Liu, L. Ye, L. Kuang, J. Yang, Y. Deng, Ag and peptide co-decorate polyetheretherketone to enhance antibacterial property and osteogenic differentiation, *Colloids Surf. B: Biointerfaces* 198 (2021), 111492.
- [48] N. Abbasi, S. Hamlet, R.M. Love, N.-T. Nguyen, Porous scaffolds for bone regeneration, *Journal of Science: Advanced Materials and Devices*, 2020.
- [49] Y. Choi, D.S. Yoon, K.-M. Lee, S.M. Choi, M.-H. Lee, K.H. Park, S.H. Han, J.W. Lee, Enhancement of mesenchymal stem cell-driven bone regeneration by resveratrol-mediated SOX2 regulation, *Aging Dis.* 10 (4) (2019) 818–833.
- [50] B. Chang, W. Song, T. Han, J. Yan, F. Li, L. Zhao, H. Kou, Y. Zhang, Influence of pore size of porous titanium fabricated by vacuum diffusion bonding of titanium meshes on cell penetration and bone ingrowth, *Acta Biomater.* 33 (2016) 311–321.
- [51] G.C. Reilly, A.J. Engler, Intrinsic extracellular matrix properties regulate stem cell differentiation, *J. Biomech.* 43 (1) (2010) 55–62.
- [52] F. Riccitello, A. De Luise, R. Conte, S. D’Aniello, V. Vittoria, A. Di Salle, A. Calarco, G. Peluso, Effect of resveratrol release kinetic from electrospun nanofibers on osteoblast and osteoclast differentiation, *Eur. Polym. J.* 99 (2018) 289–297.
- [53] L. Li, M. Yu, Y. Li, Q. Li, H. Yang, M. Zheng, Y. Han, D. Lu, S. Lu, L. Gui, Synergistic anti-inflammatory and osteogenic n-HA/resveratrol/chitosan composite microspheres for osteoporotic bone regeneration, *Bioactive Mater.* 6 (5) (2021) 1255–1266.
- [54] Y. Li, S. Dänmark, U. Edlund, A. Finne-Wistrand, X. He, M. Norgård, E. Blomén, K. Hultenby, G. Andersson, U. Lindgren, Resveratrol-conjugated poly-ε-caprolactone facilitates in vitro mineralization and in vivo bone regeneration, *Acta Biomater.* 7 (2) (2011) 751–758.
- [55] M. Zhao, S.Y. Ko, I.R. Garrett, G.R. Mundy, G.E. Gutierrez, J.R. Edwards, The polyphenol resveratrol promotes skeletal growth in mice through a sirtuin 1–bone morphogenic protein 2 longevity axis, *Br. J. Pharmacol.* 175 (21) (2018) 4183–4192.
- [56] A.K. Gosain, L. Song, P. Yu, B.J. Mehrara, C.Y. Maeda, L.I. Gold, M.T. Longaker, Osteogenesis in cranial defects: reassessment of the concept of critical size and the expression of TGF-β isoforms, *Plast. Reconstr. Surg.* 106 (2) (2000), 360–71.
- [57] C.-C. Wang, C.-H. Wang, H.-C. Chen, J.-H. Cherng, S.-J. Chang, Y.-W. Wang, A. Chang, J.-Z. Yeh, Y.-H. Huang, C.-C. Liu, Combination of resveratrol-containing collagen with adipose stem cells for craniofacial tissue-engineering applications, *Int. Wound J.* 15 (4) (2018) 660–672.
- [58] Z. Lu, S. Wang, X. Zhu, X. Yuan, Y. Zhan, Y. Li, W. Wang, Resveratrol Induces Endothelial Progenitor Cells Angiogenesis via MiR-542-3p by targeting angiopoietin-2 and involves in recanalization of venous thrombosis, *Med. Sci. Monit.* 25 (2019) 7675–7683.
- [59] F. Diomedè, G.D. Marconi, L. Fonticoli, J. Pizzicarella, I. Merciaro, P. Bramanti, E. Mazzon, O. Trubiani, Functional relationship between osteogenesis and angiogenesis in tissue regeneration, *Int. J. Mol. Sci.* 21 (9) (2020) 3242.
- [60] U. Saran, S. Gemini Piperni, S. Chatterjee, Role of angiogenesis in bone repair, *Arch. Biochem. Biophys.* 561 (2014) 109–117.